

Dielectric Dispersion and Phonon Line Shape in Gallium Phosphide

A. S. BARKER, JR.

Bell Telephone Laboratories, Murray Hill, New Jersey

(Received 30 August 1967)

The infrared and Raman spectra of GaP near the transverse and longitudinal optic phonon modes are examined in detail and fitted with an oscillator with frequency-dependent damping. Some new low-frequency combination band assignments and an arsenic impurity-mode measurement are presented. A combination band near 360 cm^{-1} causes the large frequency dependence of the damping and gives an asymmetric shape to the transverse optic mode. The new fits to this asymmetric mode revise upwards the previously accepted values of the index of refraction for frequencies below 2000 cm^{-1} .

I. INTRODUCTION

RECENT experiments utilizing forward Raman scattering in the optical-phonon region in GaP¹ have shown that it is possible to obtain accurate values of the infrared index of refraction independent of conventional infrared measurements. The Raman experiments show that the commonly accepted values of the index just below the transverse optic mode frequency are about 6% low. In addition, the Raman spectra can show the transverse and longitudinal optic mode line shapes in more detail than is possible by infrared spectroscopy. The transverse optic mode shows considerable asymmetric broadening. In the present paper the phonon spectrum of GaP has been fitted with an oscillator containing frequency-dependent damping. It is shown that such damping can reasonably be expected and does reproduce the observed transverse optic (TO) and longitudinal optic (LO) mode shapes in detail. More careful infrared measurements are analyzed to yield an index which is compatible with the asymmetric broadening and the forward Raman-scattering data. The polariton dispersion curves and other features of the dielectric response are discussed using the new oscillator fit which revises the index upwards throughout the near- and far-infrared region.

II. INFRARED DISPERSION WITH CONSTANT DAMPING

A. Dielectric Function at High Frequency

For a material like GaP with one infrared-active lattice vibration, we may often describe the dielectric properties over a wide range both above and below the frequency of the optic mode by the equation^{2,3}

$$\epsilon = \epsilon_\infty + S_0\nu_0^2 / (\nu_0^2 - \nu^2 + i\nu\gamma_0). \quad (1)$$

Here ϵ is the complex dielectric function; the index of refraction is $n = \sqrt{\epsilon}$. The constant term ϵ_∞ describes the response of the medium aside from the lattice vibrations; it reflects exciton absorptions and higher interband electronic transitions. The second term describes the

phonon resonance; the parameters S_0 , ν_0^2 , γ_0 are the strength, restoring force, and linewidth of the resonance, respectively. The set of parameters commonly used to characterize GaP at 300°K is given in the first column of Table I.⁴

The value $\epsilon_\infty = 8.46$ suggests that the index of refraction approaches $n = 2.91$ for frequencies well above the lattice frequency but not too near the first electronic transitions in the ultraviolet. Careful reflectivity measurements at $\nu = 2500\text{ cm}^{-1}$ show that the index must be 3.05 ± 0.05 , i.e., somewhat higher. A much more precise value of ϵ_∞ can be computed if we incorporate recently published index data with information on the electronic and phonon dispersion.⁵ The value of ϵ actually measured at 2500 cm^{-1} is $\epsilon(2500) = 9.090$.⁶ At this frequency the dielectric function would have flattened out at the value ϵ_∞ except for the small lowering influence of the lattice mode at much lower frequencies and the small raising influence of the electronic modes at much higher frequencies.

$$\epsilon_\infty = \epsilon(2500) - \Delta\epsilon_l - \Delta\epsilon_e, \quad (2)$$

TABLE I. Dielectric parameters for GaP at 300°K .

	Oscillator 1 ^a	Oscillator 2 $\gamma = \text{const}$	Oscillator 3 $\gamma = \text{function}$ [Eq. (4)]
ϵ_∞	8.46	9.09	9.09
S_0	1.72	1.92	2.01
$\nu_0(\text{cm}^{-1})$	366.0	366.0	363.4
$\gamma_0(\text{cm}^{-1})$	1.1	1.1	1.1
S_1	7.0×10^{-4}
ν_1	349.4
γ_1	21.
S_2	3.5×10^{-4}
ν_2	358.4
γ_2	12.6
Peak in Im(ϵ) (cm^{-1})	366.	366.	365.3
Peak in Im($1/\epsilon$) (cm^{-1})	401.5	402.8	402.2
ϵ_0	10.18	11.01	11.10

^a Reference 4.

⁴ D. A. Kleinman and W. G. Spitzer, Phys. Rev. **118**, 110 (1960).

¹ C. H. Henry and J. J. Hopfield, Phys. Rev. Letters **15**, 964 (1965).

² W. G. Spitzer and D. A. Kleinman, Phys. Rev. **121**, 1324 (1961).

³ A. S. Barker, Jr., Phys. Rev. **136**, 1290 (1964).

⁵ H. Ehrenreich, H. R. Philipp, and J. C. Phillips, Phys. Rev. Letters **8**, 59 (1962).

⁶ W. L. Bond, J. Appl. Phys. **36**, 1674 (1965).

where $\Delta\epsilon_l$ and $\Delta\epsilon_e$ are the frequency-dependent contributions of the lattice and electronic modes to the dielectric function at 2500 cm^{-1} . Using the phonon data (S_0 and ν_0) given in Table I, column 2 (to be discussed below), we evaluate Eq. (1) at $\nu=2500\text{ cm}^{-1}$ and obtain the contribution $\Delta\epsilon_l \simeq -0.043$. For the electronic modes we take the measured uv reflection spectrum⁵ which we approximate by two classical oscillator resonances with parameters [see Eq. (1)]

$$\begin{aligned} S_1(\text{uv}) &= 4, & \nu_1 &= 28\,000\text{ cm}^{-1}; \\ S_2(\text{uv}) &= 4, & \nu_2 &= 32\,000\text{ cm}^{-1}. \end{aligned}$$

These modes give $\Delta\epsilon_e \simeq +0.044$. Using these $\Delta\epsilon_l$ and $\Delta\epsilon_e$ in Eq. (2), we obtain the new value for ϵ_∞ given at the top of column 2 in Table I. It happens to be very close to the value of $\epsilon(2500)$ because the high- and low-frequency dispersion effects nearly cancel.

B. Dielectric Function near the Lattice Mode

Since ϵ_∞ is an additive constant, the new value derived above raises the index throughout the infrared region unless we find reason to lower S_0 in Eq. (1). The Lyddane-Sachs-Teller relation⁷ connects S_0 with transverse and longitudinal lattice mode frequencies ν_{t0} and ν_{l0} and ϵ_∞ in the following way⁸:

$$\nu_{l0}^2/\nu_{t0}^2 = \epsilon_\infty/(S_0 + \epsilon_\infty). \quad (3)$$

Since the frequencies of these lattice modes can be measured quite accurately, we note that our increase in ϵ_∞ can be reconciled with earlier measurements of these frequencies only by *increasing* S_0 which further raises the index for frequencies below ν_0 [Eq. (1)]. In fact, we will find below that we must raise S_0 even more than suggested by Eq. (3) because of the presence of strongly frequency-dependent damping which requires a modified Lyddane-Sachs-Teller relation. We have refitted reflectivity data in a manner similar to that described by Kleinman and Spitzer⁴ using Eq. (1). The best-fit parameters with constant damping are listed in Table I, column 2. Several derived quantities are listed in the table below the parameters. The peaks in the spectra of the imaginary part of ϵ and of $1/\epsilon$ for real frequency are close to the transverse and longitudinal phonon frequencies.⁸ ϵ_0 is the limiting value of the dielectric function at low frequency. No independent low-frequency measurement has been published for this parameter. The fit discussed in this section predicts $\epsilon_0 = 11.01$ which is about 8% larger than the earlier prediction.⁴

⁷ R. H. Lyddane, R. G. Sachs, and E. Teller, Phys. Rev. **59**, 673 (1941).

⁸ The frequencies which appear in the LST relation must be defined quite carefully when there is finite damping, i.e., when the modes have finite width (see Ref. 3). For the simple oscillator form of ϵ we are using here for GaP we may use the frequency of the peak in $\text{Im}(\epsilon)$ and of the peak in $\text{Im}(1/\epsilon)$ for ν_{t0} and ν_{l0} and have the equation hold to better than one part in 10^6 .

III. INFRARED DISPERSION WITH FREQUENCY-DEPENDENT DAMPING

A. Infrared Loss Spectrum

Figure 1 shows the attenuation coefficient α of insulating GaP measured in the region 170 to 1000 cm^{-1} . α is derived over most of the range from transmission and reflection measurements using the equation

$$T = (1-R)^2 e^{-\alpha t} / (1-R^2 e^{-2\alpha t}),$$

where T is the fractional transmission, R the bulk reflectivity, and t the sample thickness.⁴ In the region 310 to 440 cm^{-1} (i.e., near ν_{l0}), α is too large to allow transmission measurements using the thinnest samples available. In this region we have used data taken from a Kramers-Kronig analysis of reflectivity measurements. At frequencies between the two types of measurement both methods are somewhat imprecise, so small gaps have been left in the spectrum. The dashed curve in Fig. 1 gives the attenuation coefficient arising from the constant damping oscillator of Eq. (1) with the parameters of Table I, column 2. Since the damping parameter γ_0 was chosen to fit reflectivity data,⁴ we expect the loss curve to be fairly well fit by the oscillator between ν_{t0} and ν_{l0} (i.e., near 385 cm^{-1}). Figure 1 shows, however, that away from ν_{l0} the attenuation spectrum of the crystal has considerable structure arising from combination bands and, in the case of the peak at 268 cm^{-1} , from a local mode. Because the constant γ_0 can give no structure, we expect it to represent any background loss which changes very little with frequency. We note however that, even if we subtract the combination bands, the oscillator (dashed curve, Fig. 1) gives too low an attenuation for frequencies below ν_{t0} . We can improve the oscillator fit here by increasing γ_0 (the linewidth) but this would spoil the fit just above ν_{l0} . We evidently need a frequency-dependent γ_0 .

In what follows we will concern ourselves with fitting

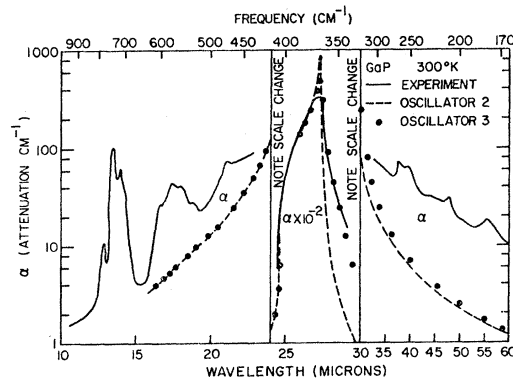


Fig. 1. Power-attenuation coefficient α for GaP. The infrared measurements are given by the solid curve. In the central region where α exceeds 100 cm^{-1} a Kramers-Kronig analysis is used to obtain the attenuation. The dashed curve and the points arise from oscillator fits.

TABLE II. Phonon frequencies (cm^{-1}) for several points in the Brillouin Zone.

Phonon Branch	Ref. 10 (300°K)			Ref. 9 (4°K)	Present Study (300°K)
	Γ	L	X	X	Γ
TA	0	64	103	106	0
LA	0	212	172 ^a	254	0
TO	366	391	379	366	365.3 ± 0.5^b
LO	404	368	358	...	402.5 ± 0.5^b
Infrared combination bands					
Predicted					
TO(L) - LA(L)	391 - 212 = 179				Observed 179
TA(X) + TA(X)	103 + 103 = 206				209
	(106 + 106 = 212 at 4°K)				
LO(X) - TA(X)	358 - 103 = 255				255
TA(X) + LA(X)	(106 + 254 = 360 at 4°K)				357 [from $\gamma(\nu)$]

^a This frequency appears low. We have used the frequency given in Ref. 9.

^b The LO-TO frequency difference is known more accurately; it is $37.2 \pm 0.2 \text{ cm}^{-1}$.

the frequency dependence of γ_0 near ν_{10} . That is, we will concentrate on the asymmetry of the ν_{10} mode but not on the combination band structure farther than about 30 cm^{-1} from ν_{10} . This more remote combination band structure could be fitted, but it has very little strength in terms of its contribution to the index of refraction. The structure in γ_0 very close to ν_{10} which we do fit does contribute significantly to the index and does control the TO mode line shape seen in Fig. 1 and in the Raman spectrum. It is our main purpose to examine these latter two features in detail. Before proceeding with the line-shape study, we can examine *a priori* reasons for the increased damping on the low-frequency side of ν_{10} .

Table II lists some phonon frequencies which might contribute to the two-phonon density of states to which a TO phonon can decay. Using the data of Ref. 9, we note that a sum band formed from the X-point TA+LA phonons should come at 360 cm^{-1} . This band could provide large damping on the low-frequency side of ν_{10} . Examining other sum and difference band possibilities^{9,10} in Table II, we find that the next higher band is well above ν_{10} . Except for accidental inflection points within the Brillouin zone we might thus expect large damping just below a somewhat broadened mode at ν_{10} while the phonon mode at ν_{10} should be quite narrow.

B. Raman Spectrum

Figure 2 shows the 90° Stokes scattering observed in GaP at 300°K using a He-Ne laser. The increased damping on the low-frequency side of ν_{10} is evident, as well as the very small linewidth of the ν_{10} lattice vibration. Since the dielectric function ϵ describes the response of the transverse lattice mode and the function $1/\epsilon$ the response of the longitudinal mode, we have plotted these functions as dashed curves for oscillator 2 in Fig. 2 for comparison with the Raman line shapes.¹¹

⁹ P. J. Dean, Phys. Rev. **157**, 655 (1967).

¹⁰ M. V. Hobden and J. P. Russell, Phys. Letters **13**, 39 (1964); J. P. Russell, J. Phys. (Paris) **26**, 629 (1965).

¹¹ For a simple model of an optic mode where both the Raman

We note that again the constant damping oscillator does not have enough damping near, and particularly just below, ν_{10} .

C. Dielectric Function with Frequency-Dependent Damping

We now proceed to allow γ_0 , the damping parameter in Eq. (1), to be frequency-dependent.

To preserve the causal form of ϵ , i.e., to have the real and imaginary parts obey the Kramers-Kronig relations, γ_0 must have both real and imaginary parts.¹² One way of obtaining a causal form and parametrizing the problem is to let the damping term be approximated by damped oscillators of the type used in Eq. (1). We

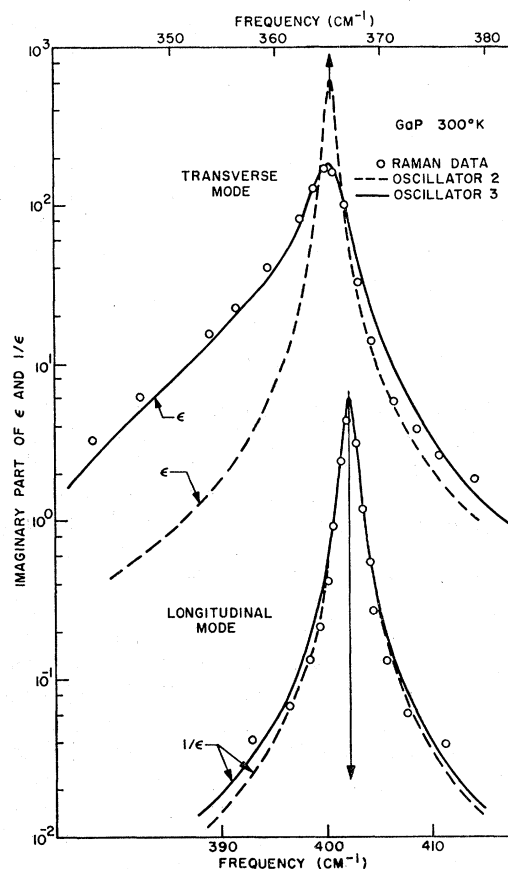


Fig. 2. Transverse and longitudinal optic mode structure in GaP. The measured Raman intensities have been scaled to fit the dielectric function of oscillator 3 near the peaks and has been corrected for instrument resolution. The dashed and solid curves are oscillator fits.

polarizability and the infrared dipole moment depend on a single coordinate, it can be shown that the Raman line shape is simply a thermal population function times the dielectric response function for the mode. In the present case we neglect the small frequency dependence of the thermal population function over the width of the modes.

¹² M. Lax, J. Phys. Chem. Solids **25**, 487 (1964).

choose the form

$$\epsilon = \epsilon_{\infty} + \frac{S_0(1 - \sum_{i=1}^n S_i)\nu_0^2}{\nu_0^2 - \nu^2 + i\nu\gamma_0 - \sum_{i=1}^n S_i\nu_i^2\nu_0^2/(\nu_i^2 - \nu^2 + i\nu\gamma_i)} \quad (4)$$

The last two terms in the denominator describe the damping; the sum is the frequency-dependent component. For $n=1$ it has a peak near ν_1 with strength S_1 and breadth γ_1 . The main peak in ϵ will usually still be near ν_0 but its breadth now depends on the value of the damping function at ν_0 . We can represent more complicated situations by adding several oscillators in the damping term. Each oscillator represents a particular combination (usually two-phonon) band in the spectrum.

The damping function also causes frequency shifts in the resonant denominator of ϵ . For example, at frequencies well below ν_0 and ν_1 , we find (for $n=1$)

$$\epsilon(\nu \sim 0) = \epsilon_{\infty} + S_0(1 - S_1)\nu_0^2/(\nu_0^2 - \nu^2 - S_1\nu_0^2). \quad (5)$$

Low-frequency measurements would suggest that the resonance should occur at $\nu_0(1 - S_1)^{1/2}$. A consideration of the high-frequency form of ϵ suggests that the resonance is at ν_0 . The actual resonance can occur above or below ν_0 depending on the parameters S_1 , ν_1 , γ_1 .

Taking the zero-frequency limit of Eq. (5), we find that

$$\epsilon_0 = \epsilon_{\infty} + S_0, \quad (6)$$

as is also predicted by Eq. (1). This results from our choice of the factor $(1 - \sum_i S_i)$ in Eq. (4) and is merely for convenience in fitting spectra.¹³ The Lyddane-Sachs-Teller relation corresponding to the dielectric function given by Eq. (5) has been discussed previously.¹⁴ For one damping mode ($n=1$) it contains two transverse and two longitudinal frequencies since once we introduce the damping as an oscillator mode we have a two-mode problem. Column 3 in Table I shows the parameters used for the fit of Eq. (4) to the GaP Raman data. Two overlapping damping modes have been used (near 349 and 358 cm^{-1}) just below the ν_{10} resonance. In attempting the fits it was quickly found that the damping mode should be asymmetric as is usually the case for the two-phonon density of states arising from simple zone boundary critical points. What is required is a slow rise on the low-frequency side and a fast falloff on the high-frequency side of the damping function. We have preferred to approximate this behavior with two oscillators rather than deal with more complicated damping functions.

D. Infrared Mode Shape

In Fig. 1 we see the fit to the infrared loss spectrum that can be achieved with Eq. (4). There is now a satisfactory fit near ν_{10} except right at the peak. We have

¹³ If we wish to discuss the temperature dependence of the damping, this factor should be omitted. The S_i are then taken to

not attempted to fit the peak to our data since the data here comes from the Kramers-Kronig analysis of the reflectivity right on top of the reststrahlen band. Our own experiments and those of others⁴ have shown that one is never sure that the maximum reflectivity has been achieved experimentally. Slightly etched surfaces always reflect more but continued etching, while it may remove more damaged surface and thereby raise the reflectivity, always leaves etch pits which in turn lower the reflectivity. Oscillator 3 (Table I, column 3) predicts a peak reflectivity of 0.952 for our particular polarization and angle of incidence. The highest reflectivity that has been measured is 0.92. The important feature in Fig. 1 is the much better fit on the steeply rising parts of the attenuation spectrum.

E. Raman Mode Shape

In Fig. 2 we show the Raman data plotted along with the appropriate dielectric functions corresponding to the new oscillator (column 3, Table I). Comparing the dashed and solid curves, we note that the oscillator with frequency-dependent damping describes the Raman line shape much more accurately. A better fit can be obtained only if an asymmetric damping function is used or if several more oscillators are used to more closely approximate the desired asymmetric function.

In Fig. 3 the real and imaginary parts of the damping function are plotted. We have added all the real parts to ν_0^2 (Eq. 4) and taken the square root to show the frequency shifts, and have added the imaginary parts to γ_0 to give the effective linewidth. From Table I we note that ν_0 is 363.4 cm^{-1} compared with the previous oscil-

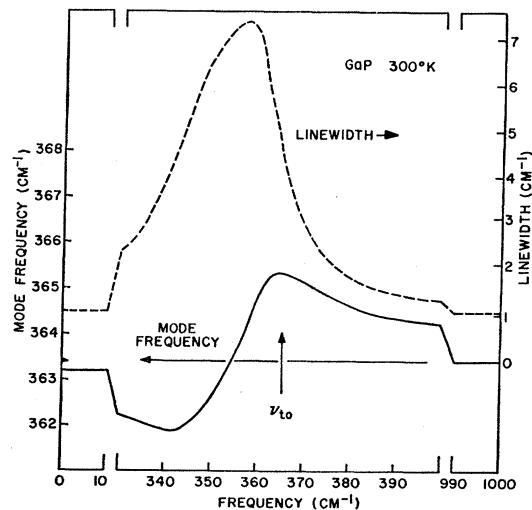


FIG. 3. Linewidth and frequency-shift functions for oscillator 3. The linewidth function (dashed curve) shows a strong asymmetric peak at 357 cm^{-1} .

be temperature-dependent with the usual Bose factors $1 + n_1 + n_2$ for sum bands and $n_1 - n_2$ for difference bands (Ref. 12).

¹⁴ A. S. Barker, Jr., in *Proceedings of the Symposium on Ferroelectricity*, Warren, Michigan, 1966 (Elsevier Publishing Co., Inc., Amsterdam, 1967).

lators where it was 366 cm^{-1} . Figure 3 shows that the damping "dresses" the restoring force causing the resonance frequency to be 365.3 near ν_{10} .

F. Infrared Index of Refraction and the Polariton Dispersion Curve

Table I shows that the limiting value of the dielectric function at very low frequencies has been raised to 11.1 (column 3) by the new fits. The complete spectrum of the index may be obtained from Eq. (4) using two terms for the damping function in the denominator and the parameters given in Table I. Henry and Hopfield have used the old index data (Table I, column 1) to predict the polariton frequencies observed by them in near-forward Raman scattering.¹ The experimental frequency^{1,15} for zero-degree scattering (307 ± 1) is considerably below the value predicted by oscillator 1. Use of a larger infrared index corrects this discrepancy. Figure 4 shows the polariton dispersion curve for the oscillators of columns 1 and 3 of Table I. Also shown is the zero-degree line that a polariton generated by Stokes scattering has to lie on if the 6328 \AA laser is used as the exciting source. The observed polariton is plotted as a point. We note that the new oscillator predicts much more closely the observed polariton frequency.

IV. DISCUSSION

In Fig. 1 we have shown the attenuation spectrum of GaP at 300°K . Most of the peaks above 400 cm^{-1} have been identified with two-phonon combination bands.⁴ The region below ν_{10} has not been explored previously. The main peak at 268 cm^{-1} we identify as an arsenic local mode. This mode has been previously detected for much higher arsenic concentration in reflectivity studies of mixed $\text{GaAs}_y\text{P}_{1-y}$ crystals.¹⁶ The present crystal was grown on a GaAs seed by vapor transport. x-ray fluorescence measurements give the As concentration as 0.1 at. % with an uncertainty of a factor of 2. On cooling to 20°K this local mode sharpens to 4.5 cm^{-1} width and the low-frequency shoulder disappears. Two other peaks appear in the attenuation spectrum at 209 and 179 cm^{-1} . The latter peak disappears almost completely on cooling to 20°K . It appears likely that this 179 cm^{-1} peak is a difference band formed from TO-LA at the L point in the Brillouin zone according to the assignments in Ref. 10. The formula for the temperature dependence of such a combination predicts a 10^{-5} times decrease in strength on cooling to 20°K which is in agreement with our data. The mode at 209 cm^{-1} we assign to TA+TA at the X point. The predicted temperature dependence is a four times decrease in intensity on cooling and this is observed. This peak also shifts its frequency from 209 to 212 cm^{-1} on cooling. This shift confirms the difference between the high- and

¹⁵ W. L. Faust and C. H. Henry, Phys. Rev. Letters **17**, 1264 (1966).

¹⁶ H. W. Verleur and A. S. Barker, Jr., Phys. Rev. **149**, 715 (1966).

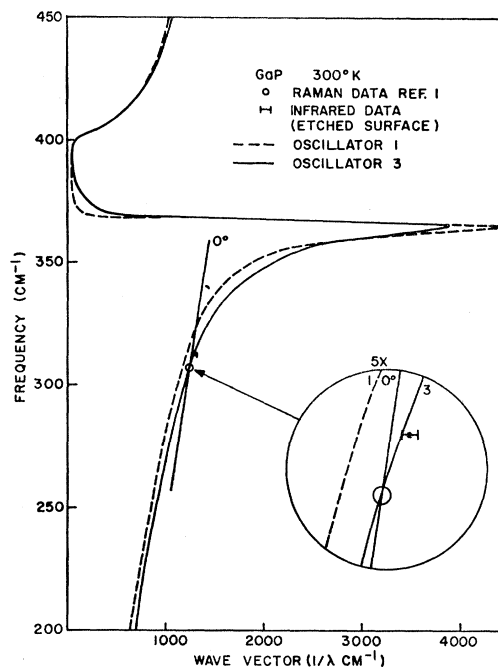


Fig. 4. Polariton dispersion curve for GaP at 300°K . The solid curve results from the best oscillator fit (oscillator 3) to the TO and LO modes using frequency-dependent damping. The experimental points are taken from Ref. 15 and from an analysis of infrared reflectivity.

low-temperature values of the fundamental TA frequency (103 and 106 cm^{-1}) shown in Table II, suggesting that the 103 cm^{-1} room-temperature value may be a little low and should be raised to 104.5 cm^{-1} . Both peaks and the 255 cm^{-1} shoulder are listed in Table II with assignments.

The main point of the present paper is the derivation of new values for the index of refraction throughout the infrared region. It must be emphasized that an accurate oscillator representation of the index must include frequency-dependent damping. In Table I we have listed in column 2 the best oscillator fit using fixed damping. This oscillator does not provide a large enough index below ν_{10} . We cannot further increase the strength of this oscillator because this causes the TO and LO peaks to spread farther apart in violation of both infrared and Raman measurements of the mode frequencies. The oscillator with frequency-dependent damping allows us to add strength just below the TO mode without shifting the TO peak. We have shown how the asymmetric infrared and Raman line shapes are consistent with a damping function peaked at 357 cm^{-1} . From Table II we find that a TA+LA combination band would come at 360 cm^{-1} at helium temperature and probably very near 357 cm^{-1} at 300°K in agreement with the frequency of the peak of our damping function. Since this combination band drops in strength about a factor of 3 on cooling below 80°K we can expect a marked decrease in the TO mode asymmetry with cooling.

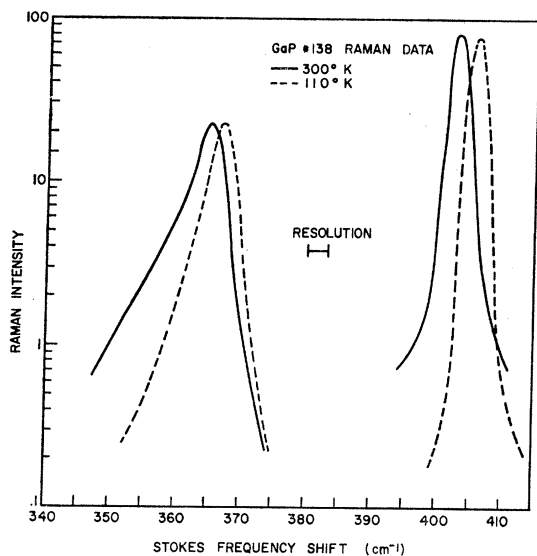


Fig. 5. Comparison to TO and LO modes at 300 and 110°K. Note reduction in asymmetry and shift to higher frequencies.

In Fig. 5 we show the 300 and 110°K Raman spectra to illustrate the temperature dependence of the mode asymmetry and frequency. On cooling to 110°K the damping mode S_1+S_2 will decrease in strength from 2.92 to 1.37 assuming we have correctly identified the components ($106+254\text{ cm}^{-1}$). The figure shows that the asymmetry caused by the damping mode is certainly reduced. Quantitative analysis would require a careful examination of the temperature dependence of γ_0 . It apparently drops also on cooling since the LO mode appears narrower at 110°K.

The reduction in S_1+S_2 can be used to calculate the TO mode frequency shift on cooling. We have already noted that S_1+S_2 dress the mode frequency ν_0 . The value of ν_0 we have been using (Table I, oscillator 3) is not a bare restoring force since it includes the effects of phonon interactions at frequencies above those with which we have been concerned. Equation (5) suggests that ν_0 could be better written

$$\nu_0 = \nu_0'(1 - S_3)^{1/2},$$

where ν_0' is the bare frequency as far as phonon interactions are concerned and S_3 represents the effects of all higher-lying multiphonon absorption bands. On cooling, S_3 will decrease, raising ν_0 . This behavior is generally to be expected in crystals; all high-frequency multiphonon bands cause the fundamental phonon frequencies to increase on cooling. The unusual feature in GaP is the S_1+S_2 band just below ν_0 . On cooling this band will have a lowering effect on ν_{10} so that the net temperature dependence is reduced. We can estimate S_3 by replacing all the multiphonon bands in the $12\text{--}22\text{-}\mu$ region (Fig. 1) by one band at $\nu_3=600\text{ cm}^{-1}$. We estimate $S_3=0.04$ from the integrated absorption strength of these bands. For the temperature dependence we take S_3 to be composed of two fundamental bands both at 300 cm^{-1} . On cooling from 300 to 110°K

TABLE III. Comparison of experimental and predicted reflectivities at 312 cm^{-1} .

$\nu = 312\text{ cm}^{-1}$	Index of refraction	Reflectivity R_p at 11.5° incidence
Oscillator 1	3.840	0.338
2	4.014	0.353
3	4.098	0.362
Sample 139		
Optical polish	...	$0.358 \pm .005$
Polish and etch	...	$0.366 \pm .005$

such a combination band will drop in strength from $S_3=0.04$ to 0.026. We then have

$$\begin{aligned} \nu_0(300^\circ\text{K}) &= 370.7(1 - 0.04)^{1/2} = 363.4, \\ \nu_0(110^\circ\text{K}) &= 370.7(1 - 0.026)^{1/2} = 366.0, \end{aligned}$$

so this effect causes a shift of 2.6 cm^{-1} .

We next consider the effect of the damping mode S_1+S_2 . S_1+S_2 decreases 2.2 times on cooling to 110°K. Figure 3 shows that such a reduction in the dispersion of the mode frequency near 365 drops ν_{10} about 1 cm^{-1} . The net shift of ν_{10} on cooling is therefore $2.6 - 1 = 1.6\text{ cm}^{-1}$ frequency increase on cooling. The shift of ν_{10} shown in Fig. 4 is in satisfactory agreement with this estimate.

From the Lyddane-Sachs-Teller relation [Eq. (3)] it can be seen that the temperature dependence of ϵ_∞ is needed along with the shifts in ν_{10} to calculate the shift of ν_{10} . Experimentally (Fig. 5) we find that ν_{10} rises about 3 cm^{-1} on cooling to 110°K.

In Fig. 4 we have shown the polariton dispersion curve derived from our fits. The main confirmation of our new value of the index near 307 cm^{-1} comes from the polariton measured in forward Raman scattering. Infrared reflectivity measurements of course measure the same dispersion. The rise of reflectivity with increasing frequency below ν_{10} is just a measure of the increasing velocity mismatch of electromagnetic waves in free space and the polariton waves in the crystal. In Table III we list our best infrared reflectivity data at 312 cm^{-1} to compare with the index given by the various oscillators in Table I. The two infrared measurements agree to within experimental uncertainty; however, we prefer the higher value given by the etched surface. This measurement confirms oscillator 3 (Table I) as giving the correct index in agreement with the polariton measurements. The lower reflectivity value lies halfway between oscillators 2 and 3 but is considerably above oscillator 1 again pointing up the incorrectness of the parameters used for the dielectric function in oscillator 1.

ACKNOWLEDGMENTS

The author has benefitted from several discussions with C. H. Henry and P. J. Dean. C. F. Frosch kindly supplied several samples of GaP. The assistance of J. A. Ditzenberger in taking the infrared data is gratefully acknowledged.